Supporting Information

Room-Temperature and Solution-Processable Cu-Doped Nickel Oxide Nanoparticles for Efficient Hole-Transport Layers of Flexible large-area Perovskite Solar Cells

Qiqi He[a], Kai Yao*[b], Xiaofeng Wang[a], Xuefeng Xia[a], Shifeng Leng[b], Fan Li*[a, c]

[a]Department of Materials Science and Engineering, Nanchang University, 999 Xuefu Avenue, Nanchang 330031, China;

[b]Institute of Photovoltaics, Nanchang University, 999 Xuefu Avenue, Nanchang 330031, China

[c]State Key Laboratory of Molecular Engineering of Polymer (Fudan University), Shanghai 200433, China

∗Corresponding authors. *E-mail address*: lfan@ncu.edu.cn (F. Li), yaokai@ncu.edu.cn (K. Yao)

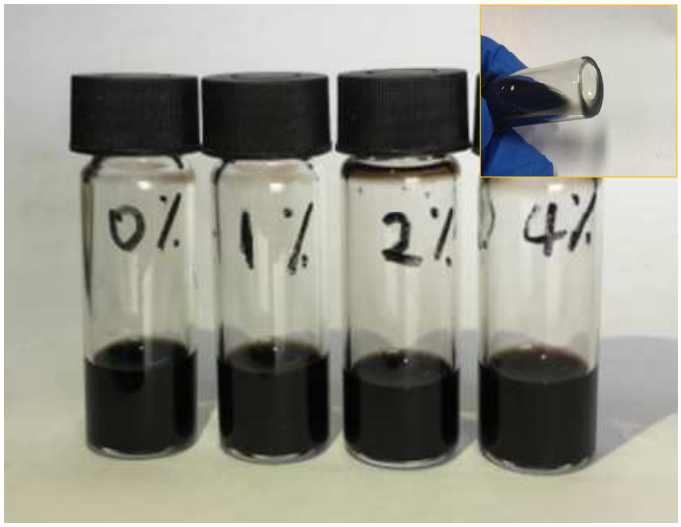

Figure S1. Photographs of the pristine and Cu-doping NiO_x NPs aqueous dispersion solutions stored in ambient environment for 30 days. The concentration of all the solutions are 20 mg mL^{-1}.

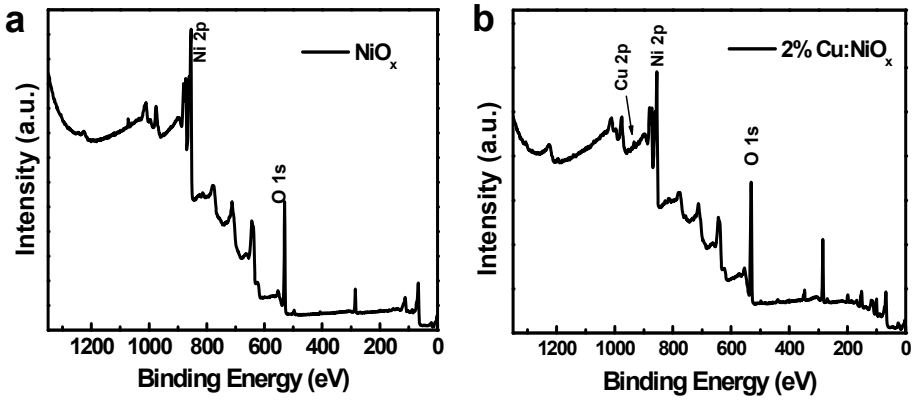

Figure S2. Wide survey XPS spectra of (a) the pristine NiO_x NPs and (b) Cu:NiO_x (2%) NPs.

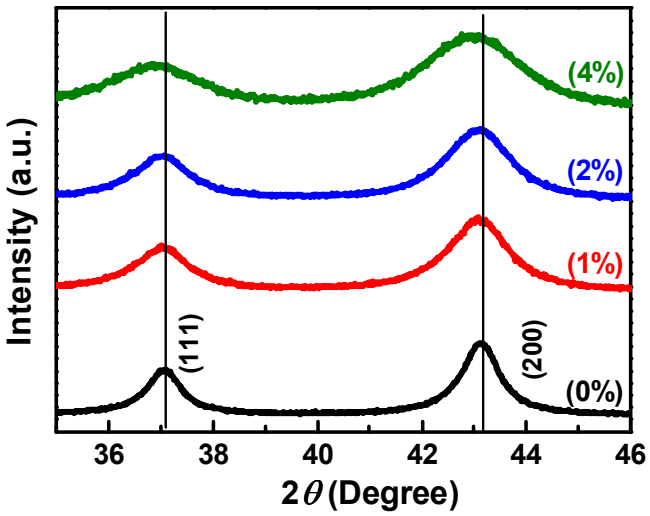

Figure S3. Enlarged XRD spectra of the pristine NiO_x and Cu:NiO_x NPs.

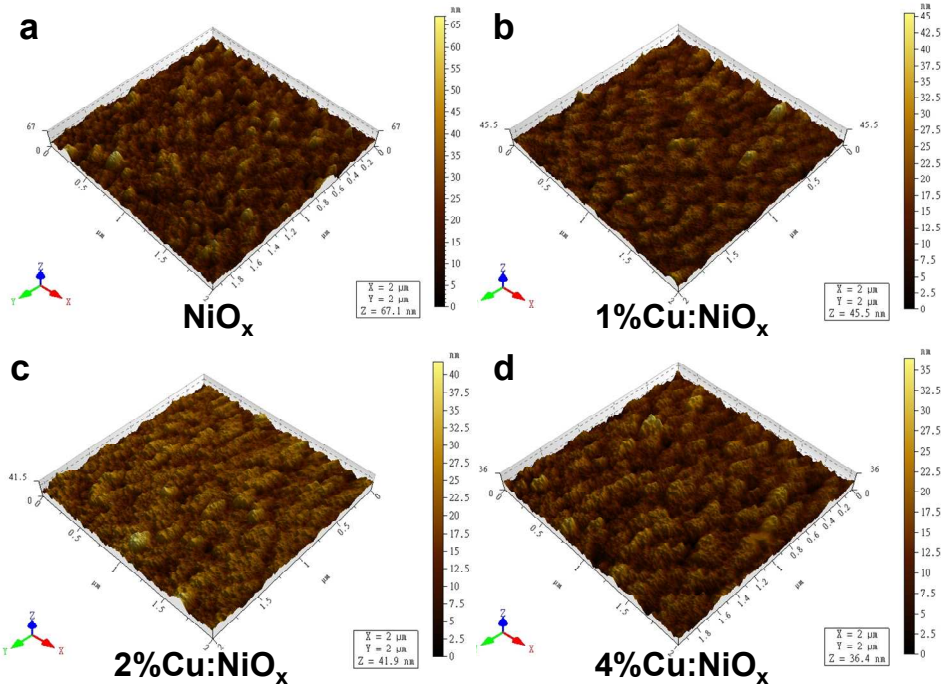

Figure S4. Three-dimensional (3D) AFM images of (a) NiO_x; (b) $Cu:NiO_x$ (1%); (c) $Cu:NiO_x$ (2%) and (d) $Cu:NiO_x$ (4%) films deposited on rigid ITO/glass substrates.

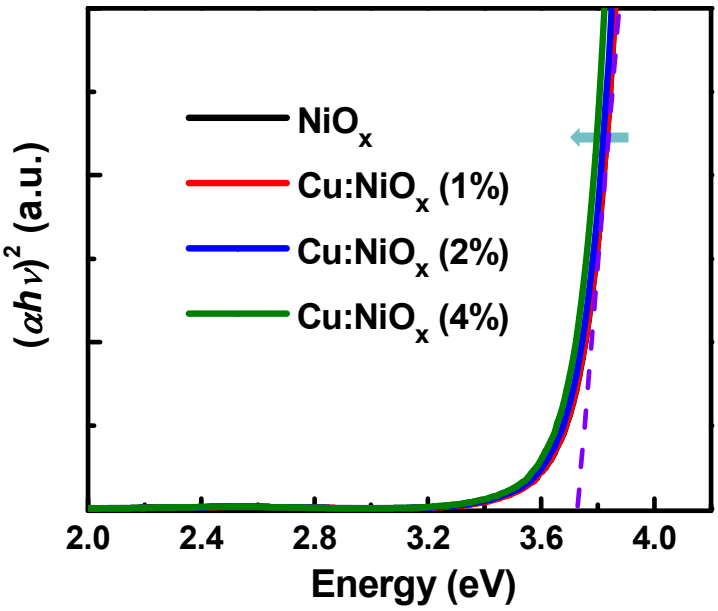

Figure S5. The Tauc plot of the pristine NiO_x and $Cu:NiO_x$ films. The direct bandgap energy (3.72 eV) of pristine NiO_x was extracted from the curves, marked by the purple broken line. Incorporation of Cu atoms slightly narrowed the bandgap.

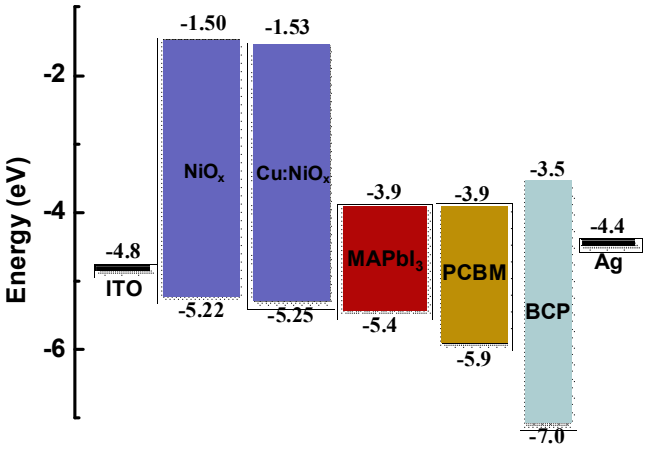

Figure S6. Energy level diagram of the PSC device.

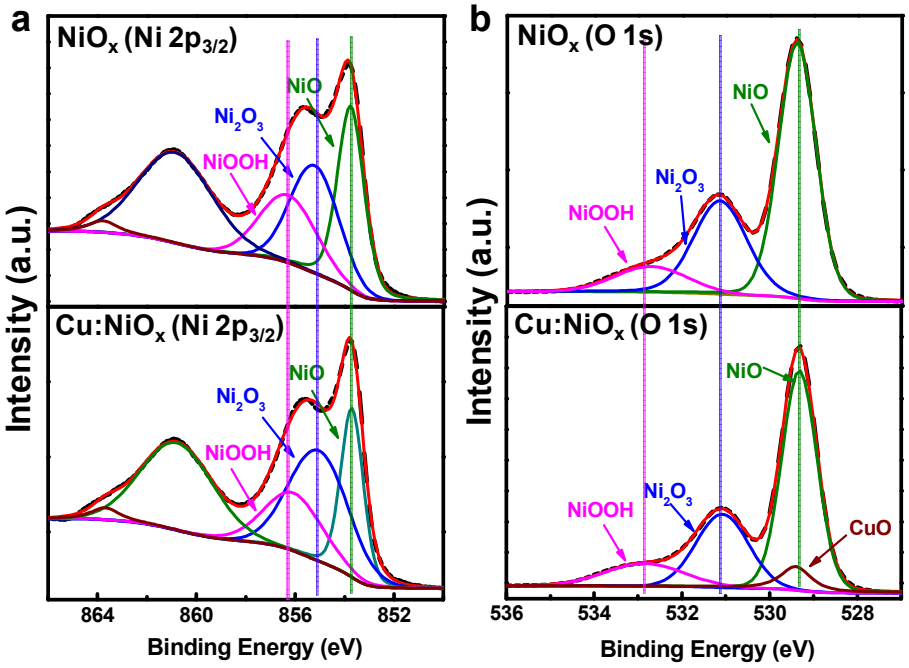

Figure S7. XPS results of NiO_x and Cu:NiO_x (2%) films (a) Ni $2p_{3/2}$ and (b) O 1s core level peaks.

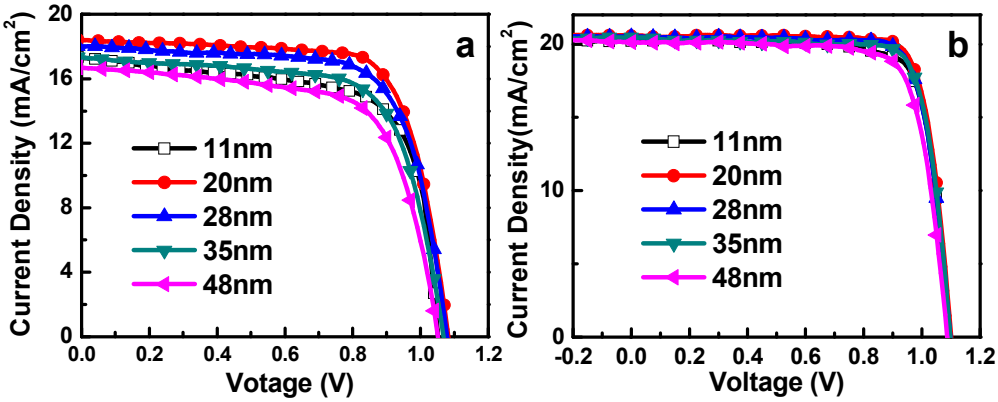

Figure S8. $J-V$ curves of (a) NiO_x-based and (b) Cu:NiO_x-based perovskite solar cells fabricated from different thicknesses of HTLs.

Table S1. Performance of perovskite devices fabricated from different thicknesses of HTLs scanned with 10 mV voltage steps and 10 ms delay times under standard AM 1.5 illumination (100 mW cm^{-2}) at small-size area (0.10 cm^2).[a]

HTLs	Thickness	J_{SC} (mA cm^{-2})	V_{OC} (V)	FF	PCE (%)	R_s (Ω cm^2)
NiO_x	11 nm	17.31 ± 1.04	1.05 ± 0.03	0.68 ± 0.04	12.35 ± 1.03	7.96
	20 nm	18.42 ± 0.65	1.08 ± 0.02	0.73 ± 0.02	14.53 ± 0.62	5.23
	28 nm	18.01 ± 0.71	1.08 ± 0.02	0.71 ± 0.02	13.81 ± 0.65	5.79
	35 nm	17.36 ± 0.75	1.07 ± 0.02	0.69 ± 0.03	12.87 ± 0.72	7.84
	48 nm	16.57 ± 0.81	1.05 ± 0.02	0.66 ± 0.03	11.48 ± 0.79	8.92
$Cu:NiO_x$	11 nm	20.22 ± 0.55	1.09 ± 0.02	0.79 ± 0.02	17.41 ± 0.68	3.43
	20 nm	20.56 ± 0.35	1.10 ± 0.01	0.80 ± 0.01	18.06 ± 0.44	2.89
	28 nm	20.51 ± 0.35	1.10 ± 0.01	0.80 ± 0.01	18.05 ± 0.45	2.92
	35 nm	20.45 ± 0.35	1.10 ± 0.01	0.79 ± 0.01	17.77 ± 0.51	3.55
	48 nm	20.12 ± 0.35	1.09 ± 0.01	0.78 ± 0.02	17.11 ± 0.59	3.81

[a]The statistics is determined from 20 devices.

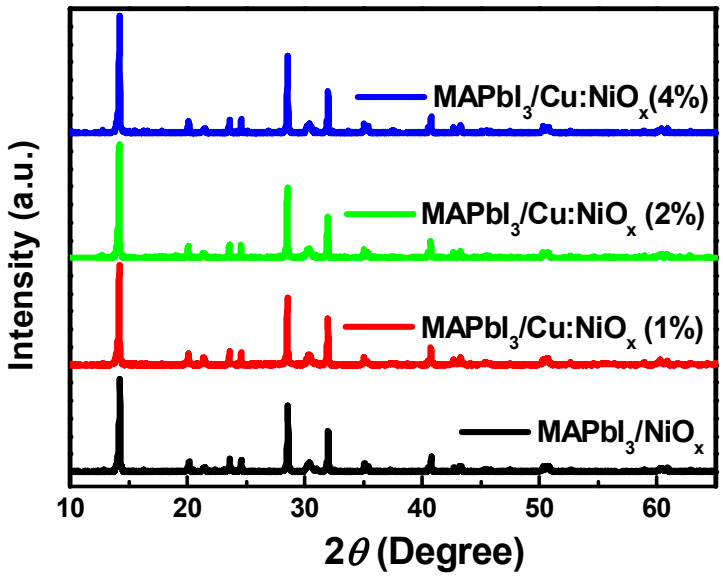

Figure S9. The XRD patterns of $MAPbI_3$ perovskite films deposited on the pristine NiO_x and $Cu:NiO_x$ films.

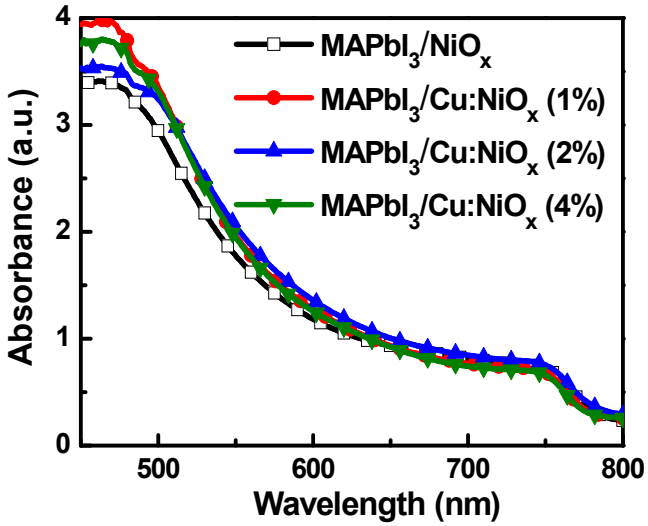

Figure S10. UV–vis absorption spectra of $MAPbI_3$ films deposited on the pristine NiO_x and $Cu:NiO_x$ films.

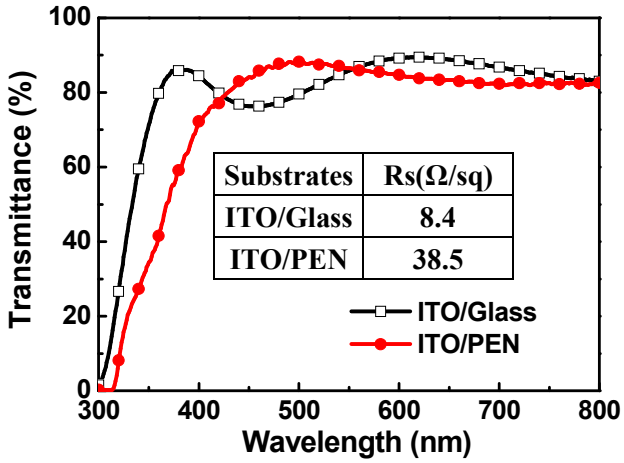

Figure S11. The optical transmission spectra of ITO/glass and ITO/PEN substrates. Inset: the square resistance of ITO/glass and ITO/PEN substrates, respectively.

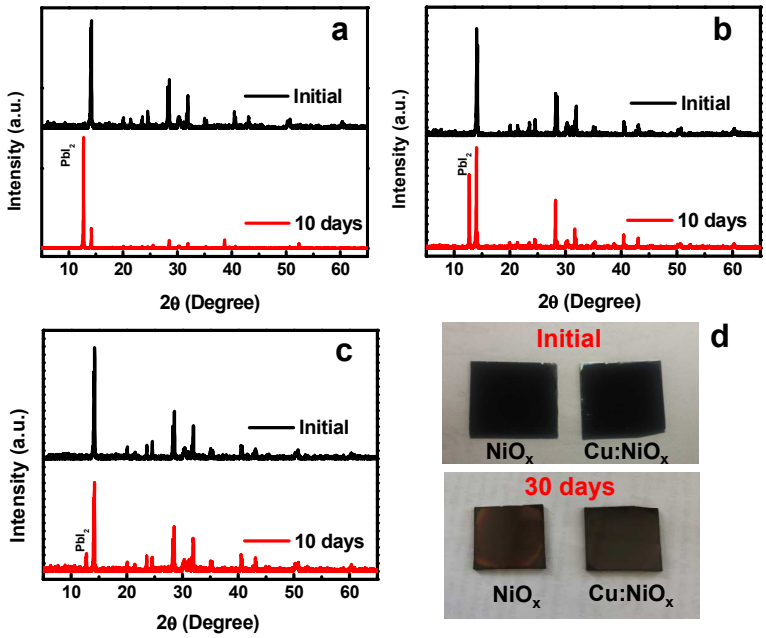

Figure S12. X-ray diffraction patterns of $MAPbI_3/PC_{71}BM$ films deposited on various HTLs: (a) PEDOT:PSS; (b) NiO_x and (c) $Cu:NiO_x$ (2%) as a function of storage time. (d) The images of $MAPbI_3/PC_{71}BM$ films deposited on various HTLs. The feature of PbI_2 phase was labeled out in the spectra.